

Subwavelength Total Acoustic Absorption with Degenerate Resonators

Min Yang,* Chong Meng,* Caixing Fu, Yong Li, Zhiyu Yang, and Ping Sheng

Department of Physics, Hong Kong University of Science and Technology, Clear Water Bay, Kowloon, Hong Kong, China

We report the experimental realization of perfect sound absorption by sub-wavelength monopole and dipole resonators that exhibit degenerate resonant frequencies. This is achieved through the destructive interference of two resonators' transmission responses, while the matching of their averaged impedances to that of air implies no backscattering, thereby leading to total absorption. Two examples, both using decorated membrane resonators (DMRs) as the basic units, are presented. The first is a flat panel comprising a DMR and a pair of coupled DMRs, while the second one is a ventilated short tube containing a DMR in conjunction with a sidewall DMR backed by a cavity. In both examples, near perfect absorption, up to 99.7%, has been observed with the airborne wavelength up to 1.2 m, which is at least an order of magnitude larger than the composite absorber. Excellent agreement between theory and experiment is obtained.

Total absorption of sound using subwavelength structures or materials has always been a challenge, since the linear dynamics of dissipative systems dictates the fractional power to be linearly proportional to the elastic deformation energy [1], which is negligible in the sub-wavelength scale. To enhance the dissipation, it is usually necessary to increase the energy density, for example, through resonances. However, in an open system, radiation coupling to resonances is an alternative that can be effective in reducing dissipation. In previous studies, by utilizing localized subwavelength resonances, membrane-type metamaterial [2–7], containing decorated membrane resonator (DMR) with tunable weights, has shown efficient and flexible capability in low frequency sound absorption [8]. A balance between dissipation and scattering at resonance has been found for optimum absorption [9]. More recently, a perfect absorber has been realized by hybridizing DMR's two resonances through coupling via a thin gas layer. Through interference, waves reflected from such DMR have been shown to completely cancel that from a reflective wall placed a short distance (about 1/133 of airborne wavelength) behind the DMR [9, 10]. Meanwhile, the coherent perfect absorber (CPA) in optics shows that the scattering waves at resonance can be cancelled when another counter-propagating coherent light wave, with specific phase and intensity, interferes with the incident beam, thereby leading to total absorption [11–16]. Recent efforts have also been made for its analogy in acoustics [17–20]. However, except for some theoretical attempts in acoustic [21] and numerical studies in optics [22], up to now no perfect absorber has been experimentally realized that intrinsically eliminates all the scattered waves, thereby realizing total absorption regardless of the incident direction, and with no need for a control wave.

In this article, we advance the idea of creating a total acoustic absorption unit comprising a monopole (symmetric under mirror reflection) and a dipole (anti-symmetric) resonator that are resonant at the same frequency. Similar to the hybrid resonance, this degenerate absorption unit can have two useful degrees of freedom, inherited from the two resonances. During a scattering event, reflection can be eliminated by making the average impedance of the two resonators to be impedance-

matched with the background medium. Transmission can also be eliminated if the response on the other side is zero due to destructive interference. The net result is a perfect absorber that scatters no sound and that does not need a reflecting back wall as in the hybrid membrane resonator (HMR) or another controlling wave as in the CPA. Owing to its subwavelength dimensions, acoustic waves incident from any direction will be completely dissipated. Below we report two such implementations based on using DMR's. In the flat panel composite absorber, a DMR dipolar resonator was built on the same panel with a pair of DMRs that are coupled by a thin layer of sealed air, which can generate a monopole resonance as well as a dipole resonance [6]. When the coupled-DMR's monopolar resonance has the same resonance frequency as the DMR, perfect absorption of sounds is observed in both numerical simulations and experiment, provided the value of the absorption coefficient is within a suitable range. In the second implementation, the ventilated composite absorber, we place a DMR in the center of a hollow tube and mount a HMR on the sidewall to generate monopolar resonance. When the HMR resonates at the same frequency of the DMR's Fano resonance [7, 23–25], perfect absorption has also been found while the air can freely flow through the tube.

The basis of understanding the perfect absorption by this type of degenerate resonators is that, for a resonator in a planar array with sub-wavelength dimension, only its surface-averaged displacement $\langle W \rangle$ over the unit cell, i.e., piston-like motion component, couples to radiative modes in air. Here, W denotes the resonator's displacement normal to the plane and the brackets denote surface averaging. The remaining component of the displacement, $\delta W = W - \langle W \rangle$, generates only evanescent waves and hence can be characterized as 'deaf'. The process of scattering sound by a DMR is thereby one-dimensional [2, 6, 10], and for time harmonic waves the impedance Z is inversely related to the Green function G , i.e., $Z = i/(\omega G)$, where $G = \langle W \rangle / \langle p \rangle$, with p denoting pressure.

For a monopole resonator and a dipole resonator placed side by side on a flat surface, the surface-averaged displacement $\langle W \rangle$ on the transmission side, for the two resonators combined, would vanish if $G_d - G_m = 0$, i.e., the two responses cancel each other through destructive interference (refer to Appendix A Here the subscripts d and m denote dipole and monopole, respectively. As the monopole resonator has two

* Contributed equally to this work

membranes oscillating out of phase, whereas the dipole resonator has only one membrane, it must be the case that the dipole resonator is out of phase of one of the monopole resonator's surface. Hence the above condition should always be possible to be satisfied. For the incident wave side, the two resonators' responses are in phase. Here the backscattering is eliminated through impedance matching to air. As $Z \equiv p/\langle \dot{W} \rangle = i/(\omega G)$, we must have $(G_m + G_d)/2 = i/(\omega Z_0)$, where Z_0 denotes the air impedance. Therefore, to completely eliminate scatterings, we should have,

$$G_m = i/(\omega Z_0) = G_d. \quad (1)$$

While the above description uses the flat composite absorber as the concrete example, exactly the same applies to the ventilated composite absorber.

The response functions in Eq. (1) can be written explicitly in terms of eigenmodes [6, 26]. In the vicinity of a monopolar resonance, the associated G_m is given by the Lorentzian form,

$$G_m = \frac{|\langle W_m^f \rangle - \langle W_m^b \rangle|^2}{2\rho_m[(\omega_m^2 - \omega^2)^2 + \omega^2\beta_m^2]} [(\omega_m^2 - \omega^2) + i\omega\beta_m], \quad (2)$$

where the superscripts f and b on W indicate the front and back surfaces, $\rho_m \equiv \int_{\Omega} \rho |W_m|^2 dV$ is a parameter related to the displacement-weighted mass density for the monopolar eigenmode W_m resonating at ω_m , ρ is the local mass density, and Ω the volume of the resonator. If we denote the viscosity coefficient of the system as η [1], the dissipation coefficient β_m in Eq. (2) is defined by [9]:

$$\beta_m = \int_{\Omega} \eta |\nabla(\delta W_m)|^2 dV / \rho_m, \quad (3)$$

where η can be treated as a fitting parameter from experimental testing. Similarly, the dipolar response G_d is given by

$$G_d = \frac{2|\langle W_d \rangle|^2}{\rho_d[(\omega_d^2 - \omega^2)^2 + \omega^2\beta_d^2]} [(\omega_d^2 - \omega^2) + i\omega\beta_d]. \quad (4)$$

Note that Eq. (1) requires both responses to be imaginary. According to Eqs. (2) and (4), this can be fulfilled when the monopole and dipole resonances are degenerate at the same frequency, so that at $\omega = \omega_m = \omega_d$, $\text{Re}(G_m) = \text{Re}(G_d) = 0$. By adjusting their dissipation coefficients $\beta_{m(d)}$, such as through the intensity of the 'deaf' components $\delta W_{m(d)}$, perfect absorption can be achieved when the two modes cancel each other at the transmission side and match the impedance of air at the backscattering direction.

Normalized to incoming wave, energy absorbed by such a composite wave absorber is given by (with details shown in Appendix A).

$$A = \frac{2\omega Z_0 \text{Im}(G_m)}{[1 + \omega Z_0 \text{Im}(G_m)]^2 + \omega^2 Z_0^2 \text{Re}(G_m)^2} + \frac{2\omega Z_0 \text{Im}(G_d)}{[1 + \omega Z_0 \text{Im}(G_d)]^2 + \omega^2 Z_0^2 \text{Re}(G_d)^2}, \quad (5)$$

which comprises two terms from the monopolar and dipolar resonances, respectively. Each term reaches a maximum of

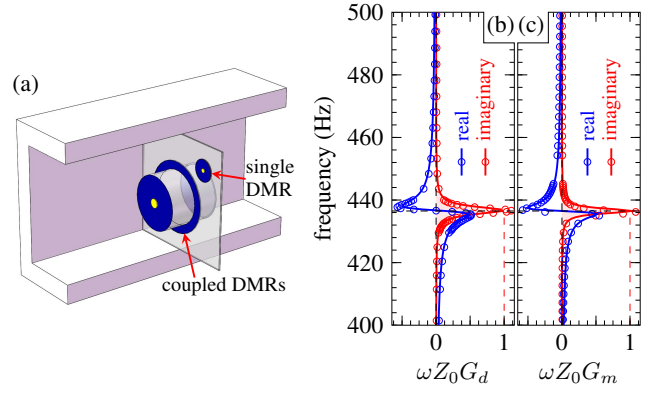


FIG. 1. (a) Schematic cutoff view of the flat panel composite absorber. Based on the parameters in Table I, the associated responses are given by Eqs. (2) and (4) as shown in (b) for the dipolar response and (c) for the monopole response. Solid curves stand for theory, and open circles are predictions based on parameters retrieved from experiments.

	#1: G_m	#1: G_d	#2: G_m	#2: G_d
α (m ² /kg)	0.031	0.043	0.11	4.93
β (Hz)	12.3	17.8	6.8	8.0
η (Pa-s)	1.14	1.18	0.95	0.722

TABLE I. Evaluated parameters for each response from numerical simulations. $\alpha = |\langle W_m^f \rangle - \langle W_m^b \rangle|^2 / (2\rho_m)$ for G_m in the flat panel composite absorber (#1), $\alpha = |\langle U_m \rangle|^2 / \rho_m$ for G_m in the ventilated composite absorber (#2), and $\alpha = 2|\langle W_d \rangle|^2 / \rho_d$ for G_d .

50% when Eq. (1) is satisfied, similar to the CPA conditions [9, 17].

Our idea of realizing such a degenerate perfect composite absorber is to assemble a monopolar and a dipolar resonator together while keeping the overall size in the subwavelength regime [27, 28]. The absorption unit in the flat panel composite absorber is a 90×90 mm panel consisting of a single DMR for dipolar resonance and a pair of coupled DMRs for monopolar resonance as shown in Fig. 1(a). Stretched on a rigid circular frame with radius of 8 mm, the single DMR is a 0.2 thick rubber membrane (blue circle) attached by a 56 mg weight (yellow button) in center. In the coupled-DMR, two 40-mm wide identical DMRs [blurred circles in Fig. 1(a)] seal a rigid cylindrical tube (gray cylinder) on the two ends. In the monopole resonance mode, the two DMRs, each with a 70 mg button attached, oscillate out of phase with each other and thereby compressing and expanding the air layer in-between. The coupled-DMR resonator is isolated from the nearby dipole resonator, situated ~1 cm away, by a ring-shaped membrane [blue ring in Fig. 1(a)]. Numerical simulations by COMSOL Multiphysics (with material parameters given in Ref. [26]) indicate a pair of almost degenerate resonances for DMR's dipole resonance at 436.7 Hz and the coupled-DMR's monopolar resonance at 436.5 Hz.

We plot the responses of the two resonators, in the form of their Green functions (normalized by ωZ_0) as functions of

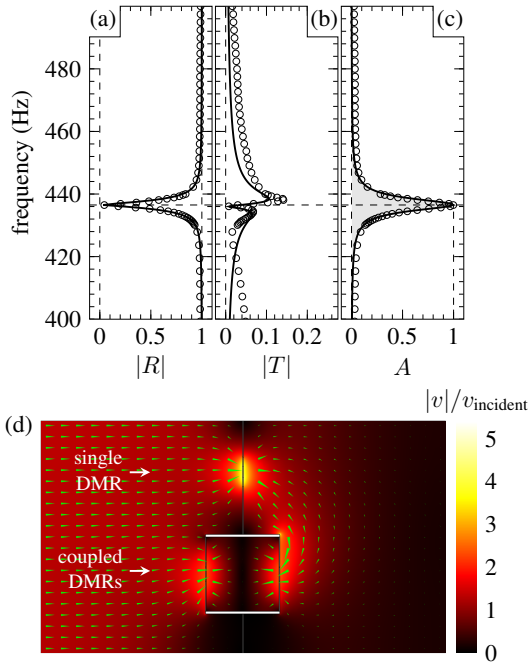


FIG. 2. (a-c) Scatterings and absorption coefficient of the flat panel composite absorber. Almost perfect absorption is seen at 436.5 Hz. The solid curves are from theory and the open circles from experiments. (d) Cross-sectional profile of air velocities at 436.5 Hz from numerical simulations. The small arrows indicate the in-plane velocity with length proportional to its magnitude. The acoustic wave is incident from the left.

frequency (solid colored curves) in Figs. 1(b,c), in which parameters in Eqs. (2) and (4) are evaluated in Table I based on simulations. By experimentally measuring the reflection R and transmission T for each resonator, their response function can also be retrieved through $\omega Z_0 G_{m(d)} = i[1 - (R \pm T)]/[1 + (R \pm T)]$ (Appendix B), as shown by open circles in Figs. 1(b,c). It should be especially noted that at the resonances, Eq. (1) has been fulfilled with $\omega Z_0 G_m = 1.133i$ and $\omega Z_0 G_d = 1.105i$, i.e., impedance matched.

In the experiment, the sample is sandwiched between two impedance tubes. With plane wave generated by the speaker at one end, scattered waves from the sample were measured by sensors mounted in the tubes on both sides of the sample. Details of measurements are shown in Appendix C. The results for this composite absorber are shown in Fig. 2. As expected, an absorption peak reaching 99.7% is seen at the degenerate resonance frequency of 436.5 Hz [Fig. 2(c)]. The associated reflection and transmission coefficients are shown in Figs. 2(a,b). Very good agreement between experiment (open circles) and theory (solid curves) is seen. The relevant airborne wavelength, 786 mm, is noted to be more than 20 times that of the absorber's thickness, and 10 times larger than its width. The simulated profile of air velocity is shown in Fig. 2(d). On the transmission side the air velocities in the vicinity of the single DMR are seen to have the opposite symmetry from that of the coupled-DMR, thereby canceling each other further away. On the incident side the plane wave

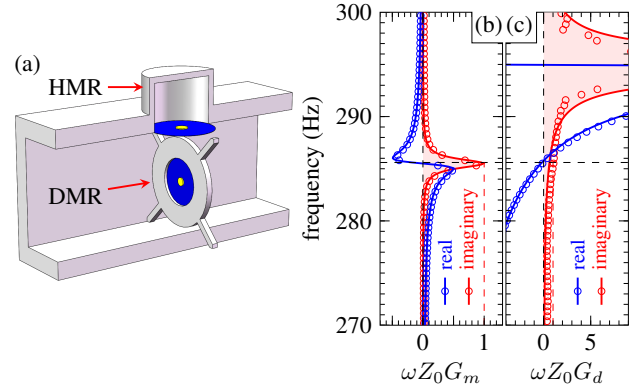


FIG. 3. (a) A schematic cutoff view of the ventilated composite absorber that comprises a sidewall monopole resonator placed in the vicinity of dipole resonator. The relevant responses are given by Eqs. (6) and (7). They are shown by solid curves in (b) for monopole sidewall resonator and in (c) for the dipolar resonator. Predictions with parameter values retrieved from experiment are shown by open circles. Very good agreement is seen. Note the Fano profile of G_d in (c)

is seen to maintain its amplitude, implying no backscattered wave owing to matched impedance.

In the ventilated composite absorber, shown in Fig. 3(a), a sub-wavelength short tube having a 90×90 mm square cross-section is seen to have a hybrid membrane resonator (HMR) attached on the sidewall. The HMR is a 35 mm deep, 55 mm wide, cylindrical chamber sealed by a rubber membrane (blue circle), with a 130 mg attached weight (yellow button). Like the sidewall Helmholtz resonator [24], the HMR generates a monopole response in air, along the tube's axial direction, through the sucking and pushing of air associated with its membrane's normal displacement. The effect on the two ports (two sides of the DMR) is proportional to $f_m/2$, where $f_m = 0.29$ is the areal ratio between the membrane and the tube's cross-sections. Similar to Eq. (2) [10], G_m is given by

$$G_m = \frac{f_m |U_m|^2 / 2}{\rho_m [(\omega_m^2 - \omega^2)^2 + \omega^2 \beta_m^2]} [(\omega_m^2 - \omega^2) + i\omega \beta_m], \quad (6)$$

where U_m is the HMR's membrane normal displacement field at the hybrid resonance with $\omega_m = 2\pi \times 285.3$ Hz. Based on the values in Table I, Eq. (6) gives the solid curves in Fig. 3(b). Experimental results (open circles) are seen to agree with the theory very well. Moreover, at the resonance frequency the data are seen to agree with the prediction of Eq. (1), with $\omega Z_0 G_m = 0.93i$.

The dipole resonator, a 40 mm-wide DMR (blue circle), is placed at the center of the square tube, with a rigid rim (gray ring) that is 8 mm in its width. The whole structure is supported by four poles [Fig. 3(a)]. We note that the membrane and its rim block the tube's cross-section with a ratio $f_d = 0.55$. While the DMR gives rise to narrow discrete resonances, the air in the remaining cross-section area contributes a smooth continuum background, with an extra term

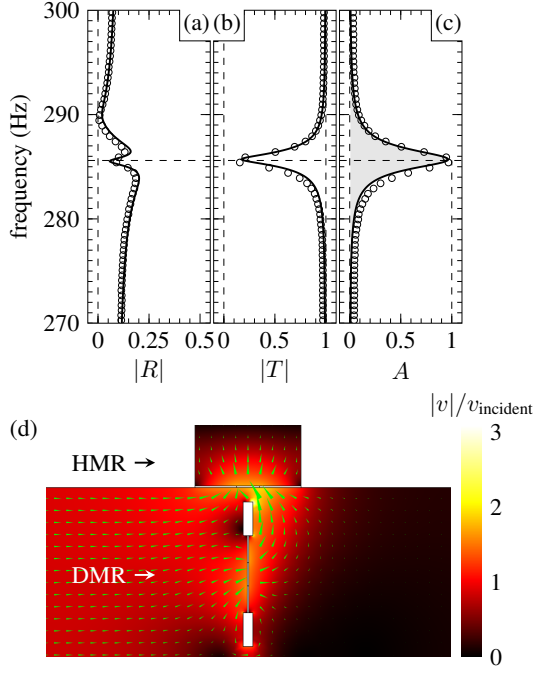


FIG. 4. (a-c) The reflection, transmission, and absorption coefficients for the ventilated composite absorber. Almost perfect absorption, reaching 99.2%, is seen at 285.6 Hz. The solid curves are from theory and the open circles from the experiments. (d) Simulated air velocities at the total absorption frequency. The green arrows are in-plane velocity with its length being proportional to the magnitude. The acoustic wave is incident from the left.

$-(1 - f_d)/(\tau\rho_0\omega^2)$ in G_d [7], so that

$$G_d = f_d \frac{2|\langle W_d \rangle|^2}{2\rho_d[(\omega_d^2 - \omega^2)^2 + \omega^2\beta_d^2]} [(\omega_d^2 - \omega^2) + i\omega\beta_d] - (1 - f_d) \frac{1}{\tau\rho_0\omega^2}. \quad (7)$$

Here τ (=8 mm) denotes width of the ring. In contrast to the Lorentzian resonance in Eq. (4), this response exhibits a distinctly asymmetric-shaped Fano resonance due to the interference between the two terms in Eq. (7), at which another zero $\text{Re}(G_d)$ exists below ω_d [7, 23–25]. To make it degenerate with the HMR, we adjust the weight on the DMR (yellow button) to be 38 mg (so that $\omega_d = 2\pi \times 295.0$ Hz). Based on the parameters in Table I, Eq. (7) yields a dipolar response (solid curves), shown in Fig. 3(c), that agrees well with the prediction obtained with experimentally retrieved parameter values (open circles). At the degenerate resonance frequency we have $\omega Z_0 G_d = 1.07i$, again agreeing with the condition given by Eq. (1) reasonably well.

The combined effect of monopole and dipole resonances is shown in Figs. 4(a-c). The composite absorber exhibits almost perfect absorption of 99.2% at 285.6 Hz, with vanishing reflection and transmission. The relevant airborne wavelength is about 1.2 m, i.e., 22 times larger than the absorber's thickness and 10 times larger than its width. Figure 4(d) shows the simulated air velocities at the peak absorption frequency.

Again, the air motion is cancelled on the transmission side, with impedance matching behavior on the incident side. It should be noted that the near-total absorption is achieved in this case while the airflow can still flow largely unimpeded in the channel.

In summary, we have shown that by combining a pair of degenerate monopole and dipole resonators with subwavelength dimensions, perfect absorption of sound can be achieved. The subwavelength dimension of the absorber unit implies that the absorption functionality is independent of the incident direction. We have experimentally demonstrated the effect by two examples: the flat panel absorber with single DMR mounted in the same panel as a coupled-DMR, and the ventilated absorber comprising a short tube with HMR mounted on its side-wall and a DMR placed in the center. Almost perfect absorption for sounds with wavelength at least 10 times larger than the absorber has been observed in both cases, with excellent agreement between theory and experiment. In addition, we would like to note that, owing to the similarity between acoustic and electromagnetic waves, the present proposed total absorption mechanism by degenerate mirror-symmetric and anti-symmetric resonances should be valid for electromagnetic waves as well, with specific polarizations.

M.Y. wishes to thank Guancong Ma for helpful discussions. This work is supported by AoE/P-02/12 from the Research Grant Council of the Hong Kong SAR government.

Appendix A: Scattering Amplitudes and Absorption Coefficient

Consider a monopole resonator at $z = 0$. It scatters plane acoustic wave incident from two sides, with two outgoing waves. With k_0 being acoustic wavevector in air, we denote the incoming waves as $p = \exp(ik_0z)$ when $z < 0$ and $p = \exp(-ik_0z)$ when $z > 0$, and the symmetric outgoing waves as $p = s_m \exp(-ik_0z)$ for $z < 0$ and $p = s_m \exp(ik_0z)$ for $z > 0$. Here s_m denotes the scattering coefficient. The resonator's monopole response on two sides can be characterized by the symmetric displacement W that is proportional to the applied pressure via the Green function G_m , i.e., $W^b = -W^f = G_m(1 + s_m)$, here the thickness of 2ϵ for the resonator is assumed to be small compared to the wavelength so that $k_0\epsilon \ll 1$. Superscripts b and f indicate back and front surfaces, respectively. From Newton's law, the amplitude of air compression (and expansion) between the two surfaces is related to pressure by the relationship $W = (\partial p / \partial z) / (\omega^2 / \rho_0)$. It follows that $W^b = -W^f = \xi(1 - s_m)$. Here ρ_0 is the density of air and $\xi \equiv i / (\omega Z_0)$, with Z_0 being the air impedance. From the continuity of displacement, the scattering coefficient s_m is given by

$$s_m = \frac{\xi - G_m}{\xi + G_m}. \quad (A1)$$

Similarly, a dipole resonator scatters the incident waves $p = \exp(ik_0z)$ for $z < 0$ and $p = -\exp(-ik_0z)$ for $z > 0$ into anti-symmetric outgoing waves with $p = s_d \exp(-ik_0z)$ for $z < 0$ and $p = -s_d \exp(ik_0z)$ for $z > 0$, where s_d is given

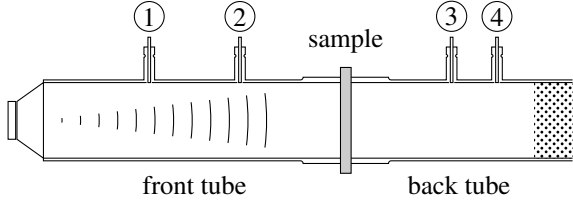


FIG. 5. Schematic illustration of the experimental apparatus. The front tube with a loudspeaker at one end has two sensors, labeled by 1 and 2, while the back tube, plugged by acoustic foam at the end, has two more sensors, as labeled by 3 and 4.

by

$$s_d = \frac{\xi - G_d}{\xi + G_d}. \quad (\text{A2})$$

For a composite resonator comprising monopole and dipole resonances with wave incident from only one side, so that $p = \exp(ik_0z)$ when $z < 0$ and $p = 0$ when $z > 0$, the reflection R can be obtained by simply superposing the two aforementioned cases:

$$R = \frac{1}{2}(s_m + s_d) = \frac{\xi^2 - G_d G_m}{(G_d + \xi)(G_m + \xi)}. \quad (\text{A3})$$

The transmission can be similarly obtained as

$$T = \frac{1}{2}(s_m - s_d) = \frac{(G_d - G_m)\xi}{(G_d + \xi)(G_m + \xi)}. \quad (\text{A4})$$

Since $A = 1 - |R|^2 - |T|^2$, the absorption coefficient A is therefore given by

$$A = \frac{2\omega Z_0 \text{Im}(G_m)}{[1 + \omega Z_0 \text{Im}(G_m)]^2 + \omega^2 Z_0^2 \text{Re}(G_m)^2} + \frac{2\omega Z_0 \text{Im}(G_d)}{[1 + \omega Z_0 \text{Im}(G_d)]^2 + \omega^2 Z_0^2 \text{Re}(G_d)^2}, \quad (\text{A5})$$

Appendix B: Retrieval of Responses from Scatterings

It is straightforward to retrieve the monopole and dipole responses, G_m and G_d , from the scattering coefficients R and T . As $s_m = R + T$ and $s_d = R - T$, the two responses can be directly solved from Eqs. (A1) and (A2):

$$G_m = \frac{1 - (R + T)}{1 + (R + T)}\xi, \quad G_d = \frac{1 - (R - T)}{1 + (R - T)}\xi. \quad (\text{B1})$$

As R and T can be measured experimentally, substituting their values into Eq. (B1) directly yields the relevant monopole and dipole responses.

Appendix C: Experiment Setup and the Measurement Method

We test the sample's scattering and absorption properties by sandwiching it between two impedance tubes having square

cross-sections. The front tube has two sensors [Fig. 5], plus a loudspeaker at the front end to generate the plane waves. The back tube has another two sensors, and the tube's back end is filled by acoustic foam to eliminate reflection. By normalizing the pressure amplitude of all the relevant sound waves by the incident sound pressure amplitude, the reflection and transmission coefficients, R and T , can be obtained from the pressure data recorded by the four sensors [9].

As scalar waves, airborne sound can propagate in a sub-wavelength waveguide without a cut-off frequency. In our experiments, the geometrical size of the apparatus (viz., the width of the square waveguide) is smaller than the relevant wavelength, so that only plane waves can propagate in both the front and back tubes [29]. The total pressure fields in the two (front and back) impedance tubes may be expressed as the sum of forward and backward waves propagating along the z direction:

$$p_1 = p_1^i e^{ik_0z} + p_1^o e^{-ik_0z}, \quad (\text{C1a})$$

$$p_2 = p_2^i e^{-ik_0z} + p_2^o e^{ik_0z}. \quad (\text{C1b})$$

Here the subscripts "1" and "2" refer to the front and back tubes, and the superscripts "i" and "o" denote the incoming and outgoing waves, respectively. To retrieve the transmission and reflection coefficients, the total pressure field should first be exactly expressed, by using the four experimentally measured parameters: p_1^i, p_1^o, p_2^i and p_2^o . Four sensors are used to determine these parameters. Two sensors labeled "1" and "2" are placed in the front tube at $z_1 = -339.5$ mm and $z_2 = -239.5$ mm, and the other two sensors labeled "3" and "4" are placed in the back tube at $z_3 = 193.0$ mm and $z_4 = 393.0$ mm [cf. Fig. 5]. Here $z = 0$ is the sample position. From Eq. (C1), the pressure values at the positions of the four sensors are

$$p(z_1) = p_1^i e^{ik_0z_1} + p_1^o e^{-ik_0z_1}, \quad (\text{C2a})$$

$$p(z_2) = p_1^i e^{ik_0z_2} + p_1^o e^{-ik_0z_2}, \quad (\text{C2b})$$

$$p(z_3) = p_2^i e^{-ik_0z_3} + p_2^o e^{ik_0z_3}, \quad (\text{C2c})$$

$$p(z_4) = p_2^i e^{-ik_0z_4} + p_2^o e^{ik_0z_4}. \quad (\text{C2d})$$

By solving Eq. (C2), we obtain

$$p_1^i = \frac{p(z_1)e^{ik_0z_1} - p(z_2)e^{ik_0z_2}}{e^{2ik_0z_1} - e^{2ik_0z_2}}, \quad (\text{C3a})$$

$$p_1^o = -\frac{p(z_1)e^{ik_0z_2} - p(z_2)e^{ik_0z_1}}{e^{2ik_0z_1} - e^{2ik_0z_2}} e^{ik_0(z_1+z_2)}, \quad (\text{C3b})$$

$$p_2^i = -\frac{p(z_3)e^{ik_0z_4} - p(z_4)e^{ik_0z_3}}{e^{2ik_0z_3} - e^{2ik_0z_4}} e^{ik_0(z_3+z_4)}, \quad (\text{C3c})$$

$$p_2^o = \frac{p(z_3)e^{ik_0z_3} - p(z_4)e^{ik_0z_4}}{e^{2ik_0z_3} - e^{2ik_0z_4}}, \quad (\text{C3d})$$

Here $p(z_j)$ is the pressure measured by each sensor labeled as " $j = 1 \sim 4$ " in the subscripts.

The scattering matrix $S(k_0)$ describing the relationship between the incoming and outgoing waves can be expressed as

$$\begin{pmatrix} p_2^o \\ p_1^o \end{pmatrix} = S(k_0) \begin{pmatrix} p_1^i \\ p_2^i \end{pmatrix}, \quad S(k_0) = \begin{pmatrix} T & R \\ R & T \end{pmatrix}. \quad (\text{C4})$$

It should be noted that, due to the symmetry of the sample in our system, the reflection and transmission coefficients R and T are identical if the sample is tuned around 180 degrees. As a result, the reflection and transmission coefficients can be

retrieved as

$$R = \frac{p_1^i p_1^o - p_2^i p_2^o}{p_1^i p_1^i - p_2^i p_2^i}, \quad (\text{C5a})$$

$$T = \frac{p_1^i p_2^o - p_1^o p_2^i}{p_1^i p_1^i - p_2^i p_2^i}. \quad (\text{C5b})$$

Here the four wave amplitude p_1^i , p_1^o , p_2^i and p_2^o are determined from Eq. (C3).

-
- [1] L. Landau and E. Lifshitz, "Theory of elasticity," (Pergamon Press, 1970) Chap. 5, p. 153.
- [2] Z. Yang, J. Mei, M. Yang, N. Chan, and P. Sheng, *Physical Review Letters* **101**, 204301 (2008).
- [3] S. H. Lee, C. M. Park, Y. M. Seo, and C. K. Kim, *Physical Review B* **81**, 241102 (2010).
- [4] C. M. Park, J. J. Park, S. H. Lee, Y. M. Seo, C. K. Kim, and S. H. Lee, *Physical Review Letters* **107**, 194301 (2011).
- [5] J. J. Park, K. Lee, O. B. Wright, M. K. Jung, and S. H. Lee, *Physical Review Letters* **110**, 244302 (2013).
- [6] M. Yang, G. Ma, Z. Yang, and P. Sheng, *Physical Review Letters* **110**, 134301 (2013).
- [7] G. Ma, M. Yang, Z. Yang, and P. Sheng, *Applied Physics Letters* **103**, 011903 (2013).
- [8] J. Mei, G. Ma, M. Yang, Z. Yang, W. Wen, and P. Sheng, *Nature Communications* **3**, 756 (2012).
- [9] M. Yang, Y. Li, C. Meng, C. Fu, J. Mei, Z. Yang, and P. Sheng, *arXiv preprint arXiv:1502.06358* (2015).
- [10] G. Ma, M. Yang, S. Xiao, Z. Yang, and P. Sheng, *Nature Materials* **13**, 873 (2014).
- [11] Y. Chong, L. Ge, H. Cao, and A. D. Stone, *Physical Review Letters* **105**, 053901 (2010).
- [12] W. Wan, Y. Chong, L. Ge, H. Noh, A. D. Stone, and H. Cao, *Science* **331**, 889 (2011).
- [13] H. Noh, Y. Chong, A. D. Stone, and H. Cao, *Physical Review Letters* **108**, 186805 (2012).
- [14] G. Nie, Q. Shi, Z. Zhu, and J. Shi, *Applied Physics Letters* **105**, 201909 (2014).
- [15] S. Li, J. Luo, S. Anwar, S. Li, W. Lu, Z. H. Hang, Y. Lai, B. Hou, M. Shen, and C. Wang, *Scientific reports* **4** (2014).
- [16] J. R. Piper and S. Fan, *ACS Photonics* **1**, 347 (2014).
- [17] P. Wei, C. Croënne, S. T. Chu, and J. Li, *Applied Physics Letters* **104**, 121902 (2014).
- [18] J. Song, P. Bai, Z. Hang, and Y. Lai, *New Journal of Physics* **16**, 033026 (2014).
- [19] X. Cai, Q. Guo, G. Hu, and J. Yang, *Applied Physics Letters* **105**, 121901 (2014).
- [20] V. Leroy, A. Strybulevych, M. Lanoy, F. Lemoult, A. Tourin, and J. H. Page, *Physical Review B* **91**, 020301 (2015).
- [21] A. Lapin, *Acoustical Physics* **49**, 731 (2003).
- [22] J. R. Piper, V. Liu, and S. Fan, *Applied Physics Letters* **104**, 251110 (2014).
- [23] C. Goffaux, J. Sánchez-Dehesa, A. L. Yeyati, P. Lambin, A. Khelif, J. Vasseur, and B. Djafari-Rouhani, *Physical Review Letters* **88**, 225502 (2002).
- [24] N. Fang, D. Xi, J. Xu, M. Ambati, W. Srituravanich, C. Sun, and X. Zhang, *Nature materials* **5**, 452 (2006).
- [25] B. Luk'yanchuk, N. I. Zheludev, S. A. Maier, N. J. Halas, P. Nordlander, H. Giessen, and C. T. Chong, *Nature materials* **9**, 707 (2010).
- [26] M. Yang, G. Ma, Y. Wu, Z. Yang, and P. Sheng, *Physical Review B* **89**, 064309 (2014).
- [27] Y. Ding, Z. Liu, C. Qiu, and J. Shi, *Physical Review Letters* **99**, 093904 (2007).
- [28] S. H. Lee, C. M. Park, Y. M. Seo, Z. G. Wang, and C. K. Kim, *Physical Review Letters* **104**, 054301 (2010).
- [29] P. M. Morse and K. U. Ingard, *Theoretical Acoustics* (Princeton University Press, Princeton, NJ, 1986).